Forward-backward asymmetry in top quark-antiquark production

V.M. Abazov,[35] B. Abbott,[73] B.S. Acharya,[29] M. Adams,[49] T. Adams,[47] G.D. Alexeev,[35] G. Alkhazov,[39]
A. Alton[a],[61] G. Alverson,[60] G.A. Alves,[2] M. Aoki,[48] M. Arov,[58] A. Askew,[47] B. Åsman,[41] O. Atramentov,[65]
C. Avila,[8] J. BackusMayes,[80] F. Badaud,[13] L. Bagby,[48] B. Baldin,[48] D.V. Bandurin,[47] S. Banerjee,[29] E. Barberis,[60]
P. Baringer,[56] J. Barreto,[3] J.F. Bartlett,[48] U. Bassler,[18] V. Bazterra,[49] S. Beale,[6] A. Bean,[56] M. Begalli,[3]
M. Begel,[71] C. Belanger-Champagne,[41] L. Bellantoni,[48] S.B. Beri,[27] G. Bernardi,[17] R. Bernhard,[22]
I. Bertram,[42] M. Besançon,[18] R. Beuselinck,[43] V.A. Bezzubov,[38] P.C. Bhat,[48] V. Bhatnagar,[27] G. Blazey,[50]
S. Blessing,[47] K. Bloom,[64] A. Boehnlein,[48] D. Boline,[70] E.E. Boos,[37] G. Borissov,[42] T. Bose,[59] A. Brandt,[76]
O. Brandt,[23] R. Brock,[62] G. Brooijmans,[68] A. Bross,[48] D. Brown,[17] J. Brown,[17] X.B. Bu,[48] M. Buehler,[79]
V. Buescher,[24] V. Bunichev,[37] S. Burdin[b],[42] T.H. Burnett,[80] C.P. Buszello,[41] B. Calpas,[15] E. Camacho-Pérez,[32]
M.A. Carrasco-Lizarraga,[56] B.C.K. Casey,[48] H. Castilla-Valdez,[32] S. Chakrabarti,[70] D. Chakraborty,[50]
K.M. Chan,[54] A. Chandra,[78] G. Chen,[56] S. Chevalier-Théry,[18] D.K. Cho,[75] S.W. Cho,[31] S. Choi,[31] B. Choudhary,[28]
S. Cihangir,[48] D. Claes,[64] J. Clutter,[56] M. Cooke,[48] W.E. Cooper,[48] M. Corcoran,[78] F. Couderc,[18]
M.-C. Cousinou,[15] A. Croc,[18] D. Cutts,[75] A. Das,[45] G. Davies,[43] K. De,[76] S.J. de Jong,[34] E. De La Cruz-Burelo,[32]
F. Déliot,[18] M. Demarteau,[48] R. Demina,[69] D. Denisov,[48] S.P. Denisov,[38] S. Desai,[48] C. Deterre,[18] K. DeVaughan,[64]
H.T. Diehl,[48] M. Diesburg,[48] P.F. Ding,[44] A. Dominguez,[64] T. Dorland,[80] A. Dubey,[28] L.V. Dudko,[37] D. Duggan,[65]
A. Duperrin,[15] S. Dutt,[27] A. Dyshkant,[50] M. Eads,[64] D. Edmunds,[62] J. Ellison,[46] V.D. Elvira,[48] Y. Enari,[17]
H. Evans,[52] A. Evdokimov,[71] V.N. Evdokimov,[38] G. Facini,[60] T. Ferbel,[69] F. Fiedler,[24] F. Filthaut,[34] W. Fisher,[62]
H.E. Fisk,[48] M. Fortner,[50] H. Fox,[42] S. Fuess,[48] A. Garcia-Bellido,[69] V. Gavrilov,[36] P. Gay,[13] W. Geng,[15, 62]
D. Gerbaudo,[66] C.E. Gerber,[49] Y. Gershtein,[65] G. Ginther,[48, 69] G. Golovanov,[35] A. Goussiou,[80] P.D. Grannis,[70]
S. Greder,[19] H. Greenlee,[48] Z.D. Greenwood,[58] E.M. Gregores,[4] G. Grenier,[20] Ph. Gris,[13] J.-F. Grivaz,[16]
A. Grohsjean,[18] S. Grünendahl,[48] M.W. Grünewald,[30] T. Guillemin,[16] F. Guo,[70] G. Gutierrez,[48] P. Gutierrez,[73]
A. Haas[c],[68] S. Hagopian,[47] J. Haley,[60] L. Han,[7] K. Harder,[44] A. Harel,[69] J.M. Hauptman,[55] J. Hays,[43] T. Head,[44]
T. Hebbeker,[21] D. Hedin,[50] H. Hegab,[74] A.P. Heinson,[46] U. Heintz,[75] C. Hensel,[23] I. Heredia-De La Cruz,[32]
K. Herner,[61] G. Hesketh[d],[44] M.D. Hildreth,[54] R. Hirosky,[79] T. Hoang,[47] J.D. Hobbs,[70] B. Hoeneisen,[12]
M. Hohlfeld,[24] Z. Hubacek,[10, 18] N. Huske,[17] V. Hynek,[10] I. Iashvili,[67] Y. Ilchenko,[77] R. Illingworth,[48] A.S. Ito,[48]
S. Jabeen,[75] M. Jaffré,[16] D. Jamin,[15] A. Jayasinghe,[73] R. Jesik,[43] K. Johns,[45] M. Johnson,[48] D. Johnston,[64]
A. Jonckheere,[48] P. Jonsson,[43] J. Joshi,[27] A.W. Jung,[48] A. Juste,[40] K. Kaadze,[57] E. Kajfasz,[15] D. Karmanov,[37]
P.A. Kasper,[48] I. Katsanos,[64] R. Kehoe,[77] S. Kermiche,[15] N. Khalatyan,[48] A. Khanov,[74] A. Kharchilava,[67]
Y.N. Kharzheev,[35] M.H. Kirby,[51] J.M. Kohli,[27] A.V. Kozelov,[38] J. Kraus,[62] S. Kulikov,[38] A. Kumar,[67] A. Kupco,[11]
T. Kurča,[20] V.A. Kuzmin,[37] J. Kvita,[9] S. Lammers,[52] G. Landsberg,[75] P. Lebrun,[20] H.S. Lee,[31] S.W. Lee,[55]
W.M. Lee,[48] J. Lellouch,[17] L. Li,[46] Q.Z. Li,[48] S.M. Lietti,[5] J.K. Lim,[31] D. Lincoln,[48] J. Linnemann,[62] V.V. Lipaev,[38]
R. Lipton,[48] Y. Liu,[7] Z. Liu,[6] A. Lobodenko,[39] M. Lokajicek,[11] R. Lopes de Sa,[70] H.J. Lubatti,[80] R. Luna-Garcia[e],[32]
A.L. Lyon,[48] A.K.A. Maciel,[2] D. Mackin,[78] R. Madar,[18] R. Magaña-Villalba,[32] S. Malik,[64] V.L. Malyshev,[35]
Y. Maravin,[57] J. Martínez-Ortega,[32] R. McCarthy,[70] C.L. McGivern,[56] M.M. Meijer,[34] A. Melnitchouk,[63]
D. Menezes,[50] P.G. Mercadante,[4] M. Merkin,[37] A. Meyer,[21] J. Meyer,[23] F. Miconi,[19] N.K. Mondal,[29]
G.S. Muanza,[15] M. Mulhearn,[79] E. Nagy,[15] M. Naimuddin,[28] M. Narain,[75] R. Nayyar,[28] H.A. Neal,[61] J.P. Negret,[8]
P. Neustroev,[39] S.F. Novaes,[5] T. Nunnemann,[25] G. Obrant[‡],[39] D. Orbaker,[69] J. Orduna,[78] N. Osman,[15]
J. Osta,[54] G.J. Otero y Garzón,[1] M. Padilla,[46] A. Pal,[76] N. Parashar,[53] V. Parihar,[75] S.K. Park,[31] J. Parsons,[68]
R. Partridge[c],[75] N. Parua,[52] A. Patwa,[71] B. Penning,[48] M. Perfilov,[37] K. Peters,[44] Y. Peters,[44] K. Petridis,[44]
G. Petrillo,[69] P. Pétroff,[16] R. Piegaia,[1] M.-A. Pleier,[71] P.L.M. Podesta-Lerma[f],[32] V.M. Podstavkov,[48] P. Polozov,[36]
A.V. Popov,[38] M. Prewitt,[78] D. Price,[52] N. Prokopenko,[38] S. Protopopescu,[71] J. Qian,[61] A. Quadt,[23] B. Quinn,[63]
M.S. Rangel,[2] K. Ranjan,[28] P.N. Ratoff,[42] I. Razumov,[38] P. Renkel,[77] M. Rijssenbeek,[70] I. Ripp-Baudot,[19]
F. Rizatdinova,[74] M. Rominsky,[48] A. Ross,[42] C. Royon,[18] P. Rubinov,[48] R. Ruchti,[54] G. Safronov,[36] G. Sajot,[14]
P. Salcido,[50] A. Sánchez-Hernández,[32] M.P. Sanders,[25] B. Sanghi,[48] A.S. Santos,[5] G. Savage,[48] L. Sawyer,[58]
T. Scanlon,[43] R.D. Schamberger,[70] Y. Scheglov,[39] H. Schellman,[51] T. Schliephake,[26] S. Schlobohm,[80]
C. Schwanenberger,[44] R. Schwienhorst,[62] J. Sekaric,[56] H. Severini,[73] E. Shabalina,[23] V. Shary,[18] A.A. Shchukin,[38]
R.K. Shivpuri,[28] V. Simak,[10] V. Sirotenko,[48] P. Skubic,[73] P. Slattery,[69] D. Smirnov,[54] K.J. Smith,[67] G.R. Snow,[64]
J. Snow,[72] S. Snyder,[71] S. Söldner-Rembold,[44] L. Sonnenschein,[21] K. Soustruznik,[9] J. Stark,[14] V. Stolin,[36]
D.A. Stoyanova,[38] M. Strauss,[73] D. Strom,[49] L. Stutte,[48] L. Suter,[44] P. Svoisky,[73] M. Takahashi,[44] A. Tanasijczuk,[1]

W. Taylor,[6] M. Titov,[18] V.V. Tokmenin,[35] Y.-T. Tsai,[69] D. Tsybychev,[70] B. Tuchming,[18] C. Tully,[66] L. Uvarov,[39] S. Uvarov,[39] S. Uzunyan,[50] R. Van Kooten,[52] W.M. van Leeuwen,[33] N. Varelas,[49] E.W. Varnes,[45] I.A. Vasilyev,[38] P. Verdier,[20] L.S. Vertogradov,[35] M. Verzocchi,[48] M. Vesterinen,[44] D. Vilanova,[18] P. Vokac,[10] H.D. Wahl,[47] M.H.L.S. Wang,[48] J. Warchol,[54] G. Watts,[80] M. Wayne,[54] M. Weber[g],[48] L. Welty-Rieger,[51] A. White,[76] D. Wicke,[26] M.R.J. Williams,[42] G.W. Wilson,[56] M. Wobisch,[58] D.R. Wood,[60] T.R. Wyatt,[44] Y. Xie,[48] C. Xu,[61] S. Yacoob,[51] R. Yamada,[48] W.-C. Yang,[44] T. Yasuda,[48] Y.A. Yatsunenko,[35] Z. Ye,[48] H. Yin,[48] K. Yip,[71] S.W. Youn,[48] J. Yu,[76] S. Zelitch,[79] T. Zhao,[80] B. Zhou,[61] J. Zhu,[61] M. Zielinski,[69] D. Zieminska,[52] and L. Zivkovic[75]

(The D0 Collaboration)

[1] *Universidad de Buenos Aires, Buenos Aires, Argentina*
[2] *LAFEX, Centro Brasileiro de Pesquisas Físicas, Rio de Janeiro, Brazil*
[3] *Universidade do Estado do Rio de Janeiro, Rio de Janeiro, Brazil*
[4] *Universidade Federal do ABC, Santo André, Brazil*
[5] *Instituto de Física Teórica, Universidade Estadual Paulista, São Paulo, Brazil*
[6] *Simon Fraser University, Vancouver, British Columbia, and York University, Toronto, Ontario, Canada*
[7] *University of Science and Technology of China, Hefei, People's Republic of China*
[8] *Universidad de los Andes, Bogotá, Colombia*
[9] *Charles University, Faculty of Mathematics and Physics,*
Center for Particle Physics, Prague, Czech Republic
[10] *Czech Technical University in Prague, Prague, Czech Republic*
[11] *Center for Particle Physics, Institute of Physics,*
Academy of Sciences of the Czech Republic, Prague, Czech Republic
[12] *Universidad San Francisco de Quito, Quito, Ecuador*
[13] *LPC, Université Blaise Pascal, CNRS/IN2P3, Clermont, France*
[14] *LPSC, Université Joseph Fourier Grenoble 1, CNRS/IN2P3,*
Institut National Polytechnique de Grenoble, Grenoble, France
[15] *CPPM, Aix-Marseille Université, CNRS/IN2P3, Marseille, France*
[16] *LAL, Université Paris-Sud, CNRS/IN2P3, Orsay, France*
[17] *LPNHE, Universités Paris VI and VII, CNRS/IN2P3, Paris, France*
[18] *CEA, Irfu, SPP, Saclay, France*
[19] *IPHC, Université de Strasbourg, CNRS/IN2P3, Strasbourg, France*
[20] *IPNL, Université Lyon 1, CNRS/IN2P3, Villeurbanne, France and Université de Lyon, Lyon, France*
[21] *III. Physikalisches Institut A, RWTH Aachen University, Aachen, Germany*
[22] *Physikalisches Institut, Universität Freiburg, Freiburg, Germany*
[23] *II. Physikalisches Institut, Georg-August-Universität Göttingen, Göttingen, Germany*
[24] *Institut für Physik, Universität Mainz, Mainz, Germany*
[25] *Ludwig-Maximilians-Universität München, München, Germany*
[26] *Fachbereich Physik, Bergische Universität Wuppertal, Wuppertal, Germany*
[27] *Panjab University, Chandigarh, India*
[28] *Delhi University, Delhi, India*
[29] *Tata Institute of Fundamental Research, Mumbai, India*
[30] *University College Dublin, Dublin, Ireland*
[31] *Korea Detector Laboratory, Korea University, Seoul, Korea*
[32] *CINVESTAV, Mexico City, Mexico*
[33] *Nikhef, Science Park, Amsterdam, the Netherlands*
[34] *Radboud University Nijmegen, Nijmegen, the Netherlands and Nikhef, Science Park, Amsterdam, the Netherlands*
[35] *Joint Institute for Nuclear Research, Dubna, Russia*
[36] *Institute for Theoretical and Experimental Physics, Moscow, Russia*
[37] *Moscow State University, Moscow, Russia*
[38] *Institute for High Energy Physics, Protvino, Russia*
[39] *Petersburg Nuclear Physics Institute, St. Petersburg, Russia*
[40] *Institució Catalana de Recerca i Estudis Avançats (ICREA) and Institut de Física d'Altes Energies (IFAE), Barcelona, Spain*
[41] *Stockholm University, Stockholm and Uppsala University, Uppsala, Sweden*
[42] *Lancaster University, Lancaster LA1 4YB, United Kingdom*
[43] *Imperial College London, London SW7 2AZ, United Kingdom*
[44] *The University of Manchester, Manchester M13 9PL, United Kingdom*
[45] *University of Arizona, Tucson, Arizona 85721, USA*
[46] *University of California Riverside, Riverside, California 92521, USA*
[47] *Florida State University, Tallahassee, Florida 32306, USA*
[48] *Fermi National Accelerator Laboratory, Batavia, Illinois 60510, USA*
[49] *University of Illinois at Chicago, Chicago, Illinois 60607, USA*
[50] *Northern Illinois University, DeKalb, Illinois 60115, USA*
[51] *Northwestern University, Evanston, Illinois 60208, USA*

[52]*Indiana University, Bloomington, Indiana 47405, USA*
[53]*Purdue University Calumet, Hammond, Indiana 46323, USA*
[54]*University of Notre Dame, Notre Dame, Indiana 46556, USA*
[55]*Iowa State University, Ames, Iowa 50011, USA*
[56]*University of Kansas, Lawrence, Kansas 66045, USA*
[57]*Kansas State University, Manhattan, Kansas 66506, USA*
[58]*Louisiana Tech University, Ruston, Louisiana 71272, USA*
[59]*Boston University, Boston, Massachusetts 02215, USA*
[60]*Northeastern University, Boston, Massachusetts 02115, USA*
[61]*University of Michigan, Ann Arbor, Michigan 48109, USA*
[62]*Michigan State University, East Lansing, Michigan 48824, USA*
[63]*University of Mississippi, University, Mississippi 38677, USA*
[64]*University of Nebraska, Lincoln, Nebraska 68588, USA*
[65]*Rutgers University, Piscataway, New Jersey 08855, USA*
[66]*Princeton University, Princeton, New Jersey 08544, USA*
[67]*State University of New York, Buffalo, New York 14260, USA*
[68]*Columbia University, New York, New York 10027, USA*
[69]*University of Rochester, Rochester, New York 14627, USA*
[70]*State University of New York, Stony Brook, New York 11794, USA*
[71]*Brookhaven National Laboratory, Upton, New York 11973, USA*
[72]*Langston University, Langston, Oklahoma 73050, USA*
[73]*University of Oklahoma, Norman, Oklahoma 73019, USA*
[74]*Oklahoma State University, Stillwater, Oklahoma 74078, USA*
[75]*Brown University, Providence, Rhode Island 02912, USA*
[76]*University of Texas, Arlington, Texas 76019, USA*
[77]*Southern Methodist University, Dallas, Texas 75275, USA*
[78]*Rice University, Houston, Texas 77005, USA*
[79]*University of Virginia, Charlottesville, Virginia 22901, USA*
[80]*University of Washington, Seattle, Washington 98195, USA*

We present a measurement of forward-backward asymmetry in top quark-antiquark production in proton-antiproton collisions in the final state containing a lepton and at least four jets. Using a dataset corresponding to an integrated luminosity of $5.4\,\mathrm{fb}^{-1}$, collected by the D0 experiment at the Fermilab Tevatron Collider, we measure the $t\bar{t}$ forward-backward asymmetry to be $(9.2 \pm 3.7)\%$ at the reconstruction level. When corrected for detector acceptance and resolution, the asymmetry is found to be $(19.6 \pm 6.5)\%$. We also measure a corrected asymmetry based on the lepton from a top quark decay, found to be $(15.2 \pm 4.0)\%$. The results are compared to predictions based on the next-to-leading-order QCD generator MC@NLO. The sensitivity of the measured and predicted asymmetries to the modeling of gluon radiation is discussed.

I. INTRODUCTION

The top quark is the heaviest observed elementary particle. As the only fermion whose mass is close to the electroweak scale, it may play a special role in electroweak symmetry breaking. So far, the measured top quark production and decay properties are consistent with predictions of the standard model (SM). Although the top quark was discovered more than 15 years ago [1, 2], the precision of many of these measurements is still limited by sample size [3], and more precise measurements may yet uncover evidence for processes beyond the SM that contain top quarks.

Quantum chromodynamics (QCD) predicts that top quark-antiquark ($t\bar{t}$) production in quark and antiquark collisions is forward-backward symmetric at leading order (LO). However, a positive asymmetry appears at higher orders. The asymmetry is such that the top quark is preferentially emitted in the direction of the incoming light quark, while the antitop quark follows the direction of the incoming antiquark [4]. At the Tevatron, interactions between valence quarks dominate $t\bar{t}$ production, so that the direction of the incoming quark almost always coincides with that of the proton. Thus, the Tevatron is well suited to studying such asymmetry.

Processes beyond the SM can modify the $t\bar{t}$ production asymmetry if, for example, axial currents contribute to s-channel production [5], or if there is an abnormal enhancement of t-channel production [6]. In D0's previous study of this asymmetry [7], we set limits on the fraction of $t\bar{t}$ events produced via a new, heavy, mediating particle in the s channel.

After analyzing datasets corresponding to about $1\,\mathrm{fb}^{-1}$ of integrated luminosity each, the D0 and CDF Collaborations found positive asymmetries that were consistent with next-to-leading order (NLO) predictions [7, 8]. The CDF Collaboration recently reported several results based on a dataset corresponding to an integrated lumi-

nosity of $5.3\,\mathrm{fb}^{-1}$ [9]. The asymmetry in one particular subset of CDF data differs by more than three standard deviations (SD) from the NLO prediction.

In this article we report a new study of forward-backward asymmetry in $t\bar{t}$ production using a dataset corresponding to an integrated luminosity of $5.4\,\mathrm{fb}^{-1}$, collected by the D0 experiment. We define the asymmetry in terms of the rapidity difference between the top and antitop quarks. The rapidity y is defined as $y\,(\theta,\beta)\,=\,\frac{1}{2}\ln\left[(1+\beta\cos\theta)\ /\left(1-\beta\cos\theta\right)\right]$, where θ is the polar angle and β is ratio of a particle's momentum to its energy. D0 uses a cylindrical coordinate system, with the z-axis pointing along the direction of the proton beam, and ϕ defined as the azimuthal angle. We employ a kinematic fitting technique to fully reconstruct the $t\bar{t}$ candidate events. The results of the kinematic fit are used to measure the reconstructed $t\bar{t}$ asymmetry. We then correct for acceptance and detector resolution to find the inclusive production asymmetry.

We also present an asymmetry based on the rapidity and charge of the electron or muon from a top quark decay. This method is less dependent on detector resolution than full $t\bar{t}$ event reconstruction and is sensitive to the underlying production asymmetry, thus providing a valuable cross check.

Finally, we discuss the predicted dependence of the asymmetry on gluon radiation. We verify the modeling of this radiation using the transverse momentum of the $t\bar{t}$ system.

II. D0 DETECTOR

D0 is a multipurpose detector designed to identify leptons, photons, and jets. The central tracking system, consisting of a silicon microstrip tracker and a central fiber tracker, is located within a 1.9 T superconducting solenoidal magnet [10]. Tracks of charged particles can be reconstructed for pseudorapidities $|\eta| < 2.5$. Central and forward preshower detectors are positioned in front of the calorimeter cryostats. Electrons, photons, and hadronic jets are identified using a liquid-argon and uranium calorimeter, which has a central section covering $|\eta|$ up to ≈ 1.1, and two end sections that extend coverage to $|\eta| \approx 4.2$ [11]. Muons are identified within $|\eta| < 2$, using a muon system consisting of a layer of tracking detectors and scintillation counters located in front of 1.8 T iron toroids, followed by two similar layers after the toroids [12]. The luminosity is measured using plastic scintillator arrays placed in front of the endcap calorimeter cryostats.

To identify b jets, we construct a neural network that combines variables characterizing the properties of secondary vertices and of tracks with large impact parameters relative to the primary $p\bar{p}$ interaction vertex (PV) [13]. The b-tagging requirement used in this analysis has an efficiency of about 70% for identifying b jets originating from top quark decay, and a misidentification probability of about 8% for light flavored jets associated with the production of W bosons.

III. EVENT SELECTION AND RECONSTRUCTION

We select $t\bar{t}(X) \rightarrow W^+bW^-\bar{b}(X)$ events, where one W boson decays to $q\bar{q}'$ and the other decays to $l\bar{\nu}_l$. We select electrons and muons, which may arise directly from the $W \rightarrow l\bar{\nu}_l$ decay or through an intermediate τ lepton. This $t\bar{t}$ decay chain is referred to as the l+jets channel.

The experimental signature of the l+jets channel is one isolated lepton with large transverse momentum (p_T), a significant imbalance in transverse momentum ($\not{E}_T$) from the undetected neutrino, and four or more jets: two from the $W \rightarrow q\bar{q}'$ decay and the other two from fragmentation of the b quarks. We refer to the top quark that decayed to $bq\bar{q}'$ as the "hadronic" top and to the other top quark as the "leptonic" top. Either of these terms can refer to the top quark or the antitop quark. The electric charge of the lepton identifies the electric charge of the leptonic top. The hadronic top is assumed to have the opposite charge.

A. Event Selection

The event selection criteria used in this article are similar to those used to measure the $t\bar{t}$ production cross section in the l+jets channel [14]. The reconstruction and identification of jets, leptons, and $\not{E}_T$ is described in Ref. [15]. The e+jets and μ+jets channels have similar event selection requirements. Events are triggered by requiring either a lepton (e or μ) or a lepton and a jet. To select e+jets events we require:

- one isolated electron with $p_T > 20\,\mathrm{GeV}$ and $|\eta| < 1.1$,

- $\not{E}_T > 20\,\mathrm{GeV}$, and

- $\Delta\phi(e,\not{E}_T) > (2.2 - 0.045 \cdot \not{E}_T/\mathrm{GeV})$ radians.

For μ+jets events, we impose the following criteria:

- one isolated muon with $p_T > 20\,\mathrm{GeV}$ and $|\eta| < 2.0$,

- $25\,\mathrm{GeV} < \not{E}_T < 250\,\mathrm{GeV}$,

- $\Delta\phi(\mu,\not{E}_T) > (2.1 - 0.035 \cdot \not{E}_T/\mathrm{GeV})$ radians, and

- $(p_T^\mu + \not{E}_T)^2 - (p_x^\mu + \not{E}_x)^2 - (p_y^\mu + \not{E}_y)^2 < (250\,\mathrm{GeV})^2$, where the indices x and y refer to the two coordinates in the plane transverse to the beams.

The last requirement is designed to suppress the contribution from mismeasured muon momentum associated with large $\not{E}_T$. We also veto events with a second isolated electron or muon in the final state.

Events with at least four jets, each with $p_T > 20\,\text{GeV}$ and $|\eta| < 2.5$, are accepted for further analysis. The leading jet, i.e., the jet of highest p_T, is required to have $p_T > 40\,\text{GeV}$. As in Ref. [14], we minimize the effect of multiple collisions in the same bunch crossing by requiring that jets have at least two tracks within the jet cone pointing back to the PV. We also require that at least one of the four leading jets is identified as a b jet.

The main background after this event selection is from the production of W bosons in association with jets (W+jets). There is a small contribution from multijet (MJ) production, where jets are misidentified as leptons. Other small backgrounds from single top quark and diboson production are insignificant for this analysis [7]. We use the MC@NLO event generator [16] combined with HERWIG showering [17] to model the behavior of $t\bar{t}$ events, and ALPGEN [18] combined with PYTHIA [19] to simulate the W+jets background. The events generated by the Monte Carlo (MC) programs are passed through the D0 detector simulation [10] and the same reconstruction that was used for data. To model energy depositions from noise and additional $p\bar{p}$ collisions within the same bunch crossing, data from random $p\bar{p}$ crossings are overlaid over the simulated events. The properties of the MJ background are evaluated using control samples from D0 data.

B. Kinematic reconstruction

The kinematic characteristics of each $t\bar{t}$ event are determined from the decay products through a constrained kinematic fit to the $t\bar{t}$ hypothesis [20]. In the kinematic fit, the energies and angles of the detected objects are varied and the most likely jet–parton assignment is identified by minimizing a χ^2 function based on the experimental resolution. Since the resolution on $\not{E}_T$ is much worse than on any other reconstructed object, we do not include a constraint from $\not{E}_T$ in the χ^2 calculation. In the fit, the lepton momentum and $\not{E}_T$, as well as energies of two of the jets, are constrained to combine to objects with invariant masses of $80.4\,\text{GeV}$, the mass of W boson. Additionally, the invariant masses of the hadronic and leptonic top quark candidates, each a combination of detected objects, are constrained to be $172.5\,\text{GeV}$ [21].

The four leading jets are considered in the kinematic fit. The b-tagging information is used to reduce the number of jet assignments considered in the kinematic fit by requiring that a b-tagged jet can only be assigned to b quarks from top quark decay.

We retain the events in which the kinematic fit converges and further analyze the most likely jet–parton assignment for each event. The kinematic fit converges more than 99% of the time. It identifies the correct assignment in $\approx 70\%$ of the simulated events where each quark from $t\bar{t}$ decay yields one of the jets considered in the kinematic fit. The distribution of the minimal χ^2 is presented in Fig. 1(a) and shows good agreement between data and simulation.

C. Defining the asymmetries

We define the difference in rapidities between the top quark and antitop quark,

$$\Delta y = y_t - y_{\bar{t}} = q_l(y_{t,\text{lep}} - y_{t,\text{had}}), \qquad (1)$$

where q_l is the charge of the lepton, and $y_{t,\text{lep}}$ ($y_{t,\text{had}}$) is the rapidity of the leptonic (hadronic) top quark. The corresponding forward-backward asymmetry is:

$$A_{\text{FB}} = \frac{N_{\text{F}} - N_{\text{B}}}{N_{\text{F}} + N_{\text{B}}}, \qquad (2)$$

where N_{F} is the number of "forward" events with $\Delta y > 0$, and N_{B} is the number of "backward" events with $\Delta y < 0$. The rapidity difference is invariant under boosts along the beam axis, and A_{FB} corresponds to the asymmetry in the $t\bar{t}$ rest frame.

In addition, we consider an asymmetry based on the charge and rapidity (y_l) of the electron or muon originating from the W boson from top quark decay:

$$A_{\text{FB}}^l = \frac{N_{\text{F}}^l - N_{\text{B}}^l}{N_{\text{F}}^l + N_{\text{B}}^l}, \qquad (3)$$

where N_{F}^l is the number of events that have $q_l y_l > 0$, and N_{B}^l is the number of events with $q_l y_l < 0$.

The numbers of events and the asymmetries can be defined at the "production level", yielding the generated, inclusive asymmetries that are comparable to the QCD calculations. They can also be defined after event selection and reconstruction: we report the "raw" numbers of forward and backward data events before background subtraction, and also the "reconstruction level" $t\bar{t}$ asymmetries.

IV. THE PREDICTED STANDARD MODEL ASYMMETRIES

As the asymmetry first appears at order α_s^3 of the strong coupling, with the largest contribution due to a loop diagram, it is not fully simulated by tree-level event generators. In addition, the modeling of selection and reconstruction effects requires that the production of all long-lived particles is fully simulated. The MC@NLO event generator is well suited for this measurement as it couples an NLO calculation of $t\bar{t}$ production with subsequent parton showers to fully simulate $t\bar{t}$ events. Its predictions for the asymmetry are listed in Table I.

The asymmetries predicted by MC@NLO are smaller at the reconstruction level due to several effects. The event selection has a higher efficiency for events with $\Delta y < 0$ than for those with $\Delta y > 0$, lowering A_{FB}. Due to the correlation between A_{FB} and A_{FB}^l, the acceptance also lowers A_{FB}^l. Finally, the limited experimental resolution on Δy reduces $|A_{\text{FB}}|$.

TABLE I. Predictions from MC@NLO.

Level	Channel	A_{FB} (%)	A_{FB}^l (%)
Production	l+jets	5.0 ± 0.1	2.1 ± 0.1
Reconstruction	e+jets	2.4 ± 0.7	0.7 ± 0.6
	μ+jets	2.5 ± 0.9	1.0 ± 0.8
	l+jets	2.4 ± 0.7	0.8 ± 0.6

V. MEASURING THE RECONSTRUCTED A_{FB}

The procedure for estimating the background and measuring A_{FB} is similar to the one used in Ref. [7]. To estimate the amount of background from W+jets production, we define a "likelihood" [22] discriminant using variables that are modeled well by our simulation, provide separation between signal and W+jets events, and do not bias $|\Delta y|$ for the signal. The last criterion is specific to the A_{FB} measurements, as many of the common variables used to discriminate between $t\bar{t}$ production and W+jets production are biased towards central events, and therefore towards small $|\Delta y|$ values that are less suited for this measurement.

Figure 1 shows the distributions of the four variables chosen as inputs to the discriminant. The amounts of $t\bar{t}$, W+jets, and MJ background shown in the figures are taken from the fit described below.

The composition of the data sample and the reconstructed A_{FB} are extracted simultaneously using a maximum likelihood fit to the distributions of the discriminant and sgn(Δy). The following four samples are used to construct the templates for the fit:

- simulated $t\bar{t}$ events with $\Delta y > 0$ (the t quark is reconstructed as more forward than the $\bar{t}$ quark),

- simulated $t\bar{t}$ events with $\Delta y < 0$ (the $\bar{t}$ quark is reconstructed as more forward than the t quark),

- simulated W+jets events,

- a control data sample that has been enriched in MJ production by inverting the lepton isolation requirements [14].

The distribution of the discriminant is the same for both $t\bar{t}$ templates. The normalization of the MJ background is evaluated using data based on the probability of a jet to satisfy the lepton quality requirements [14]. The likelihood maximized in the fit relates the relative normalization of the first two templates to A_{FB}, so that the fitted A_{FB} describes the reconstruction level asymmetry after background subtraction.

Table II summarizes the results of maximum likelihood fits to the full dataset and to several subsamples selected based on lepton flavor and on the number of jets in the event. Templates are derived separately for each subsample. The distributions of the discriminant are shown in Fig. 2 and the distribution of Δy is shown in Fig. 3.

The fitted asymmetries are higher than predicted in all of these samples, except for the $l+\geq 5$ jet sample.

Contributions from physics beyond the SM can modify the dependence of A_{FB} on the kinematics of the $t\bar{t}$ system. For example, the presence of a heavy mediator in the s channel of $t\bar{t}$ production could enhance the dependence of the A_{FB} on the invariant mass of the $t\bar{t}$ system ($m_{t\bar{t}}$), while contributions from t-channel production [23] and from box diagrams could also enhance its dependence on $|\Delta y|$.

The recent CDF measurement [9] found an enhanced asymmetry in regions with high $m_{t\bar{t}}$ and in regions with large $|\Delta y|$. MC@NLO predicts that the asymmetry is enhanced for high $m_{t\bar{t}}$ and for large $|\Delta y|$, but by amounts that are small compared to the current experimental precision. In Table III we summarize our measurement of these dependencies. We do not find any statistically significant dependencies.

VI. MEASURING THE PRODUCTION A_{FB}

In the previous section we discussed the measurement of the $t\bar{t}$ asymmetry at the reconstruction level. This quantity is necessarily detector specific, which makes the interpretation of the result as well as comparison to theory and to other experiments problematic. It is therefore desirable to infer the asymmetry at the production level by correcting for ("unfolding") the effects of detector resolution and acceptance on the observed asymmetry.

Only the numbers of events produced with positive and negative Δy are relevant for the calculation of the asymmetry. The migration of events within these categories, due to the finite experimental resolution in Δy, does not affect the reconstructed asymmetry. Thus, to present the result in terms of the $t\bar{t}$ production asymmetry requires an accurate correction of the migration across the boundary ($\Delta y = 0$). The importance of this correction grows with the fraction of events that fall within the detector resolution of the boundary. For Δy this fraction is $\approx 20\%$, to be contrasted with $\approx 10\%$ for the rapidity of the hadronic top quark as used in Ref. [9], and with $\approx 0.1\%$ for the lepton rapidity.

We first bin the distributions of Δy at the production and reconstruction levels. The migrations from one Δy bin to another are described through a two-dimensional matrix, and the acceptance through a diagonal matrix. To accurately describe the migration between events with positive and negative Δy, it is desirable to have fine binning in the region where the probability to misreconstruct the sign of Δy changes rapidly, that is, near $\Delta y = 0$ [7]. Fine binning is less important at large $|\Delta y|$. Coincidentally, the large $|\Delta y|$ region has lower statistics both in data and simulation, thereby limiting the precision of the migration matrix, which is derived from simulated events. To reduce this effect, we use bins of variable size, increasing towards large $|\Delta y|$. We bin the Δy distribution in 50 bins at the reconstruction level and in 26 bins
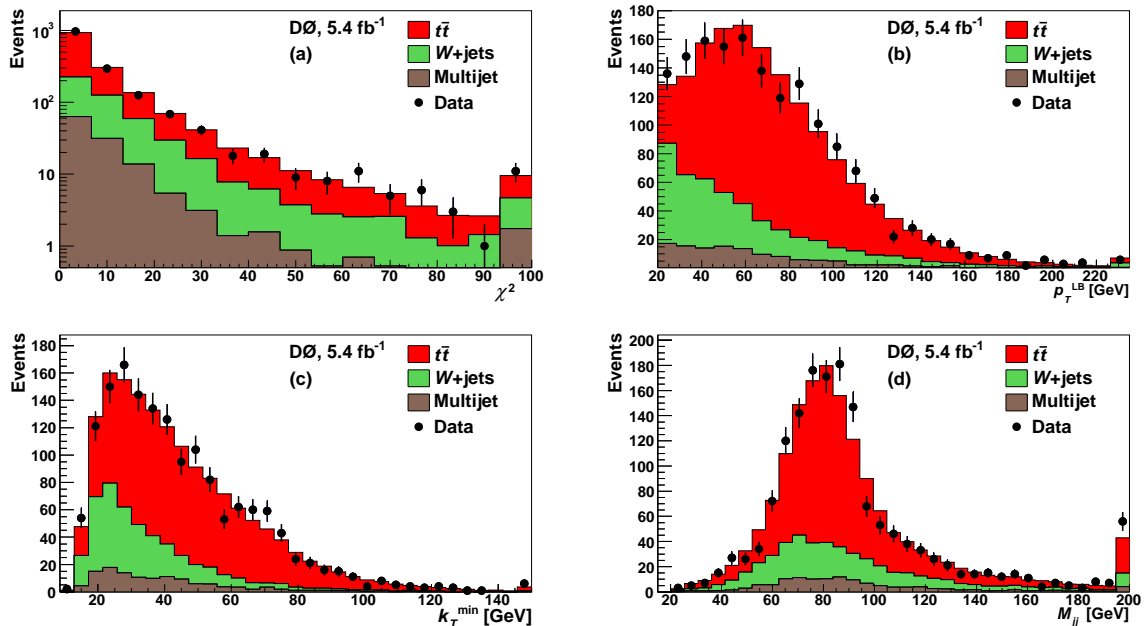
FIG. 1. Input variables to the discriminant between $t\bar{t}$ and background events. (a) χ^2 of the solution chosen by the constrained kinematic fit, (b) transverse momentum of the leading b-tagged jet, (c) $k_T^{\min} = \min\left(p_T^1, p_T^2\right) \cdot \Delta R^{12}$, where ΔR^{12} is the distance in the η-ϕ plane between the two closest jets, and p_T^1 and p_T^2 are their transverse momenta, (d) the invariant mass of the jets assigned to the $W \to q\bar{q}'$ decay in the kinematic fit, calculated using kinematic quantities before the fit. Overflows are added to the highest bins.

TABLE II. Numbers of events in data, results of fits for sample composition and A_{FB}, and predictions for A_{FB}. The asymmetries are given at reconstruction level, with their total uncertainties. The sample compositions are given with the fit uncertainties.

	$l+\geq 4$ jets	$e+\geq 4$ jets	$\mu+\geq 4$ jets	$l+4$ jets	$l+\geq 5$ jets
Raw N_{F}	849	455	394	717	132
Raw N_{B}	732	397	335	597	135
$N_{t\bar{t}}$	1126 ± 39	622 ± 28	502 ± 28	902 ± 36	218 ± 16
$N_{W+\mathrm{jets}}$	376 ± 39	173 ± 28	219 ± 27	346 ± 36	35 ± 16
N_{MJ}	79 ± 5	56 ± 3	8 ± 2	66 ± 4	13 ± 2
$A_{\mathrm{FB}}(\%)$	9.2 ± 3.7	8.9 ± 5.0	9.1 ± 5.8	12.2 ± 4.3	-3.0 ± 7.9
MC@NLO A_{FB} (%)	2.4 ± 0.7	2.4 ± 0.7	2.5 ± 0.9	3.9 ± 0.8	-2.9 ± 1.1

TABLE III. Reconstruction-level A_{FB} by subsample.

	A_{FB} (%)	
Subsample	Data	MC@NLO
$m_{t\bar{t}} < 450\,\mathrm{GeV}$	7.8 ± 4.8	1.3 ± 0.6
$m_{t\bar{t}} > 450\,\mathrm{GeV}$	11.5 ± 6.0	4.3 ± 1.3
$|\Delta y| < 1.0$	6.1 ± 4.1	1.4 ± 0.6
$|\Delta y| > 1.0$	21.3 ± 9.7	6.3 ± 1.6

at the production level.

In general, unfolding histograms where the bin width is smaller than the experimental resolution is unstable with respect to statistical fluctuations in the data. Regularization techniques are employed to suppress such fluctuations by smoothing the unfolded results [24].

We find the generated Δy distribution using a regularized unfolding, and then summarize this distribution into the A_{FB} observable according to Eq. 2. The unfolding is implemented using the TUNFOLD software [25], which we modified to account for variable bin widths.

In References [8, 9] the need for an explicit regularization is avoided by using wide bins in Δy with boundaries at $\Delta y = -3, -1, 0, 1,$ and 3. The unfolding then reduces to inverting a 4-by-4 matrix. This implicit regularization averages out migrations (and acceptance) in the wide Δy range of each bin, with the disadvantage that the migration across the $\Delta y = 0$ boundary is under-estimated for events near $\Delta y = 0$ while it is over-estimated for events near the outer edges of the central bins.

Since the regularization suppresses the badly-measured components of the data, it can also suppress part of the
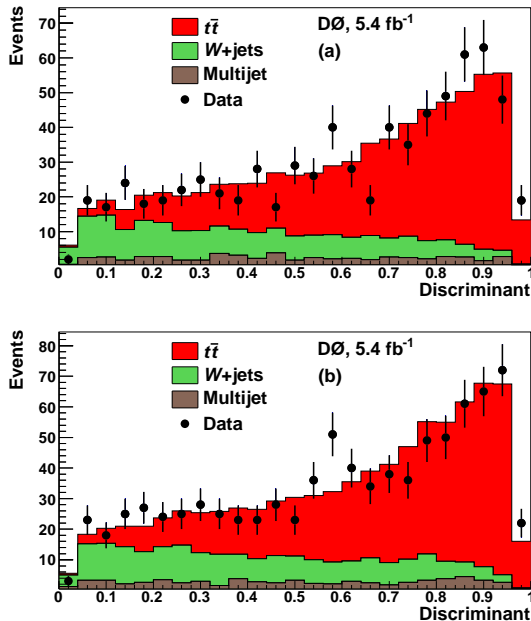
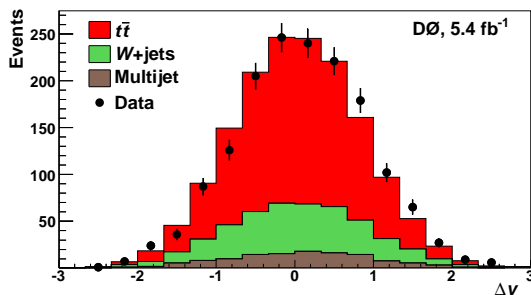FIG. 2. The discriminant for events with (a) $\Delta y < 0$ and (b) $\Delta y > 0$.

FIG. 3. The reconstructed Δy. Bin widths correspond to about half of the detector resolution in Δy.

$t\bar{t}$ production asymmetry. We calibrate the unfolding using ensembles of pseudo-datasets (PDSs). Each PDS is generated including signal and background contributions and is unfolded using the same procedure as for D0 data. We use the Δy distribution of $t\bar{t}$ events predicted by MC@NLO and a wide variety of distributions inspired by the scenarios beyond the SM, which were listed in the introduction. We choose a regularization strength that balances the statistical strength of the measurement and its model dependence. We find that the unfolded asymmetries are smaller than the input values by a multiplicative factor of 0.93 ± 0.05, where the uncertainty covers the various scenarios with $A_{\mathrm{FB}} > 5\%$ and the SM scenario. All values and uncertainties given for the unfolded A_{FB} are corrected for this bias, and the uncertainty in this factor is propagated to the result.

We estimate the statistical uncertainty on the unfolded asymmetry from its RMS in an ensemble based on the MC@NLO prediction. The regularized fine-bin unfolding

results in a statistical uncertainty on A_{FB} of 6.0%, while the coarse-bin matrix inversion technique [8, 9] results in a statistical uncertainty of 7.7%. The results of the fine-bin unfolding are given in Table IV. For comparison, the 4-bin unfolding procedure yields $A_{\mathrm{FB}} = (16.9 \pm 8.1)\%$, with the statistical and systematic uncertainties combined.

TABLE IV. Δy-based asymmetries.

| | A_{FB} (%) | |
	Reconstruction level	Production level
Data	9.2 ± 3.7	19.6 ± 6.5
MC@NLO	2.4 ± 0.7	5.0 ± 0.1

The difference between measured and predicted asymmetries at the production level has a statistical significance that corresponds to 2.4 SD, while it is 1.9 SD at the reconstruction level. Given the SM hypothesis, the probability to have this or a larger difference in significance between the reconstruction and production levels is 43%.

VII. MEASURING THE LEPTON-BASED ASYMMETRY

An alternative to measuring and unfolding A_{FB} is to measure the asymmetry A_{FB}^{l}, defined in Eq. 3. The procedure to measure A_{FB}^{l} at the reconstruction level is identical to that for A_{FB}. Figure 4 shows the distribution of $q_l y_l$. In simulated $t\bar{t}$ events, the correlation between $q_l y_l$ and the reconstructed Δy is 38%. Background subtraction is performed using a fit for events selected with an additional requirement of $|y_l| < 1.5$, as described below. The results of the fit are given in Table V.
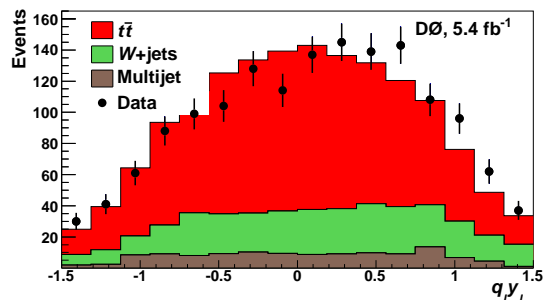

FIG. 4. The reconstructed charge-signed lepton rapidity.

Lepton reconstruction offers excellent angular resolution and accurate determination of electric charge, making migrations and their corrections negligible. By measuring this observable we therefore avoid the complications encountered in measuring A_{FB}, due to significant migration in Δy.

Correcting for detector effects thus reduces to weighting each $q_l y_l$ bin by an acceptance factor, which is the

TABLE V. Numbers of events in data, results of fits for sample composition and $A_{\rm FB}^l$, and predictions for $A_{\rm FB}^l$. The asymmetries are given at reconstruction level, with their total uncertainties. The sample compositions are given with the fit uncertainties.

	$l+\geq 4$ jets	$e+\geq 4$ jets	$\mu+\geq 4$ jets	$l+4$ jets	$l+\geq 5$ jets
Raw $N_{\rm F}^l$	867	485	382	730	137
Raw $N_{\rm B}^l$	665	367	298	546	119
$N_{t\bar{t}}$	1096 ± 39	622 ± 28	474 ± 27	881 ± 36	211 ± 16
$N_{W+\rm jets}$	356 ± 39	173 ± 28	198 ± 27	323 ± 36	31 ± 16
$N_{\rm MJ}$	79 ± 5	56 ± 3	8 ± 2	66 ± 4	14 ± 2
$A_{\rm FB}^l$ (%)	14.2 ± 3.8	16.5 ± 4.9	9.8 ± 5.9	15.9 ± 4.3	7.0 ± 8.0
MC@NLO $A_{\rm FB}^l$ (%)	0.8 ± 0.6	0.7 ± 0.6	1.0 ± 0.8	2.1 ± 0.6	-3.8 ± 1.2

TABLE VI. Lepton-based asymmetries.

	$A_{\rm FB}^l$ (%)	
	Reconstruction level	Production level
Data	14.2 ± 3.8	15.2 ± 4.0
MC@NLO	0.8 ± 0.6	2.1 ± 0.1

inverse of the selection probability. Acceptance drops rapidly for $1.1 < |y_l| < 2$, where coverage is available only in the muon channel. To avoid a large spread in the weights, which would increase the statistical uncertainty, we measure $A_{\rm FB}^l$ using only events with $|y_l| < 1.5$.

We correct for acceptance in 48 equally-spaced bins, and the results are presented in Table VI. As in the previous section, statistical uncertainties are obtained from ensembles generated according to MC@NLO predictions.

VIII. SYSTEMATIC UNCERTAINTIES

We consider multiple sources of systematic uncertainty. We vary the modeling according to the evaluated uncertainty on each source and then propagate the effect to the final result. Systematic uncertainties from different sources are added in quadrature to yield the total systematic uncertainties. In Tables VII and VIII we list the systematic uncertainties in the following categories:

Jet reconstruction (reco): This includes the jet reconstruction and identification efficiencies, as well the efficiency of the two tracks requirement described in Sec. III. We also include the effect of the multiple $p\bar{p}$ collisions within the same bunch crossing that can yield additional jets. The efficiencies in simulation are set equal to those measured in data using a dijet sample.

Jet energy measurement: The jet energy scale (JES) is measured using dijet and photon+jet samples [26]. The simulated jet energy resolution (JER) is calibrated using Z+jet data.

Signal modeling: Modeling of gluon radiation and color reconnection can affect the dependence of the

asymmetry on the transverse momentum of the $t\bar{t}$ system ($p_T^{t\bar{t}}$), as the extra radiation can differ between forward and backward events. This can affect the measured asymmetry through the sensitivity of the acceptance to $p_T^{t\bar{t}}$. MC@NLO predicts that $A_{\rm FB}$ depends on $p_T^{t\bar{t}}$, and to evaluate this uncertainty, we consider the possibility that $A_{\rm FB}$ does not depend on $p_T^{t\bar{t}}$. The effects of the finite Monte Carlo statistics and of the modeling of the detector are also taken into account.

***b* tagging:** The b-tagging efficiency and mis-tagging probability, which are determined from data, affect both the overall selection efficiency and how often the correct jet assignment is found in the kinematic fit.

Charge identification (ID): The simulated rate of misidentification of lepton charge is calibrated using $Z \to ll$ samples of same and opposite charge leptons.

Background (Bg) subtraction: The amounts of $W+$ jets and MJ background to be subtracted are changed within their fitted uncertainties. Uncertainties on the normalization of the MJ background also arise from the uncertainties on the lepton selection rates, which are used to evaluate the MJ background. The rate of inclusive $Wc\bar{c}$ and $Wb\bar{b}$ production predicted by ALPGEN must be scaled up by a factor of 1.47 to match the lepton+jets data [14]. The uncertainty on this scale factor is estimated to be 15%. The effects of the finite Monte Carlo statistics are also taken into account.

Unfolding bias: As described in Sec. VI.

IX. CROSS CHECKS

A. Checks of the asymmetries simulated for W+jets background

The measured $t\bar{t}$ asymmetries depend on the input asymmetries of the W+jets background, which are taken

TABLE VII. Systematic uncertainties on A_{FB}.

| | Absolute uncertainty [a] (%) | | |
| | Reconstruction level | | Prod. level |
Source	Prediction	Measurement	Measurement
Jet reco	±0.3	±0.5	±1.0
JES/JER	$+0.5$	-0.5	-1.3
Signal modeling	±0.3	±0.5	$+0.3/-1.6$
b tagging	-	±0.1	±0.1
Charge ID	-	$+0.1$	$+0.2/-0.1$
Bg subtraction	-	±0.1	$+0.8/-0.7$
Unfolding Bias	-	-	$+1.1/-1.0$
Total	$+0.7/-0.5$	$+0.8/-0.9$	$+1.8/-2.6$

[a] Only uncertainties above 0.1% are listed.

TABLE VIII. Systematic uncertainties on A_{FB}^{l}.

| | Absolute uncertainty [a] (%) | | |
| | Reconstruction level | | Prod. level |
Source	Prediction	Measurement	Measurement
Jet reco	±0.3	±0.1	±0.8
JES/JER	$+0.1$	-0.4	$+0.1/-0.6$
Signal modeling	±0.3	±0.5	$+0.2/-0.6$
b tagging	-	±0.1	±0.1
Charge ID	-	$+0.1$	$+0.2/-0.0$
Bg subtraction	-	±0.3	±0.6
Total	±0.5	±0.7	$+1.0/-1.3$

[a] Only uncertainties above 0.1% are listed.

from the simulation. The production of W bosons is asymmetric and strongly correlated with $q_l y_l$. However, the correlation with Δy is weaker, as Δy is reconstructed under the $t\bar{t}$ hypothesis. As this hypothesis does not match the W+jets events, the production asymmetry is reduced. To study the W+jets background, we use events with no b-tagged jets, which are enriched in W+jets production. Their simulation matches data well, as shown in Fig. 5.

To confirm that the asymmetries reconstructed for W+jets events are properly simulated, we measure these asymmetries in data as follows. Instead of selecting only events with at least one b-tagged jet, we also select events without a b-tagged jet, and divide the selected events into those with 0, 1, and ≥ 2 b-tagged jets. We then perform a simultaneous fit to these samples, with the asymmetry in the W+jets background as an additional fit parameter. Some of the observables used in the fit are defined assuming that there is a b-tagged jet. For the 0-tag sample those are calculated by treating the leading jet as though it were b tagged. The fitted W+jets asymmetries, $A_{\mathrm{FB}} = (4.1 \pm 4.1)\%$ and $A_{\mathrm{FB}}^{l} = (15.1 \pm 4.1)\%$, are in agreement with the simulated values of $A_{\mathrm{FB}} = (1.8 \pm 1.4)\%$ and $A_{\mathrm{FB}}^{l} = (14.3 \pm 1.4)\%$ (all uncertainties are statistical).
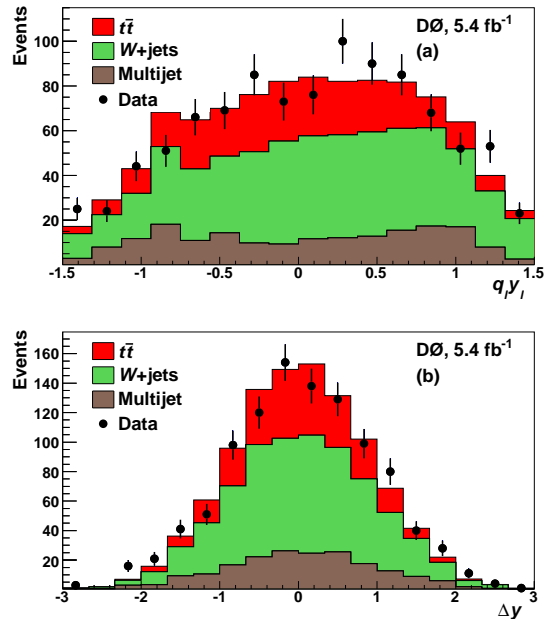

FIG. 5. The reconstructed (a) $q_l y_l$ and (b) Δy in events with no b-tagged jets. In (b), the bin widths correspond to about half of the detector resolution in Δy.

B. Dependence on magnet polarities

The polarities of the D0 magnets, both the solenoid and toroid, are regularly and independently switched to minimize the potential impact of differences in detector acceptance and efficiency for positive and negative particles. With fixed magnet polarities, localized detector problems may produce a bias, especially for A_{FB}^{l}. We find no significant differences between A_{FB}^{l} values measured in subsamples with different solenoid and toroid polarities.

C. Dependence on lepton charge

We measure A_{FB}^{l}, at reconstruction level, separately for events with positive and negative lepton charge. We find $A_{\mathrm{FB}}^{l} = (12.7 \pm 5.5)\%$ for events where the lepton charge is positive and $A_{\mathrm{FB}}^{l} = (15.6 \pm 5.0)\%$ for events where the lepton charge is negative (all uncertainties are statistical).

X. RESULTS AND DISCUSSION

Tables IV and VI summarize our measurements of the Δy- and lepton-based asymmetries at the reconstruction and production levels. The measurements are significantly higher than the MC@NLO-based predictions.

Within the SM, the $t\bar{t}$ production asymmetry first arises at order α_s^3 as a result of interference of several

production diagrams. At this order, interference of the Born and box diagrams results in positive asymmetry in two-body production, while negative contributions to the asymmetry arise from $t\bar{t}g$ production. Thus, the asymmetry is likely to show a dependence on variables that indicate the presence of extra gluons, in particular the multiplicity and kinematics of additional jets. As shown in Table II, the asymmetry in the lepton+4 jets subsample is observed to be positive, while its most likely value is negative in the lepton+$\geq$5 jets subsample.

An extra parton does not always result in the reconstruction of an extra jet, which is required to exceed a prescribed energy threshold, and be within the acceptance of the detector. In particular, a gluon emitted by an initial-state parton is likely to be too forward and/or too soft to be registered as a jet. The transverse momentum of the $t\bar{t}$ system, on the other hand, is sensitive to both soft and hard gluon radiation. Low values of $p_T^{t\bar{t}}$ correspond predominantly to two-body production, while regions of large $p_T^{t\bar{t}}$ correspond to three-body diagrams, which do not necessarily produce an extra reconstructed jet. The dependence of the asymmetry on the presence of an extra jet has been studied in the literature [27], but we are not aware of studies of a dependence on $p_T^{t\bar{t}}$.

As shown in Fig. 6, some event generators predict that the $t\bar{t}$ production asymmetry has a strong dependence on $p_T^{t\bar{t}}$, while others do not. In particular, this dependence is present in PYTHIA tunes that force an angular coherence between the top quarks and the initial state parton showers (with the MSTP(67) parameter). We account for this possible dependence in the systematic uncertainties on the measured asymmetries due to signal modeling.
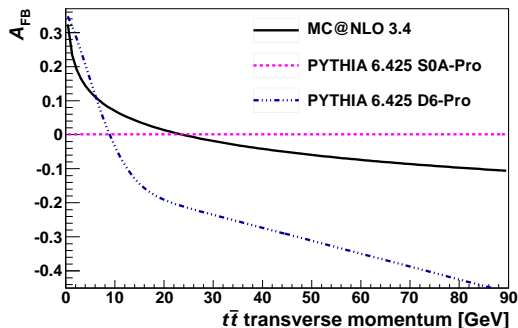

FIG. 6. The $t\bar{t}$ asymmetry versus $p_T^{t\bar{t}}$ as predicted by MC@NLO+HERWIG. For comparison, the predictions from PYTHIA with different tunes [28] are also shown.

As the predicted asymmetry may be sensitive to the modeling of gluon radiation, we examine $p_T^{t\bar{t}}$ in data. Figure 7(a) shows that the $p_T^{t\bar{t}}$ spectrum is softer in data than in the MC@NLO-based model, indicating less gluon emission. To verify this hypothesis, we simulate $t\bar{t}$ events using PYTHIA with initial state radiation (ISR) turned off. This unrealistic scenario, presented in Fig. 7(b), is in better agreement with the data. Together with the fact
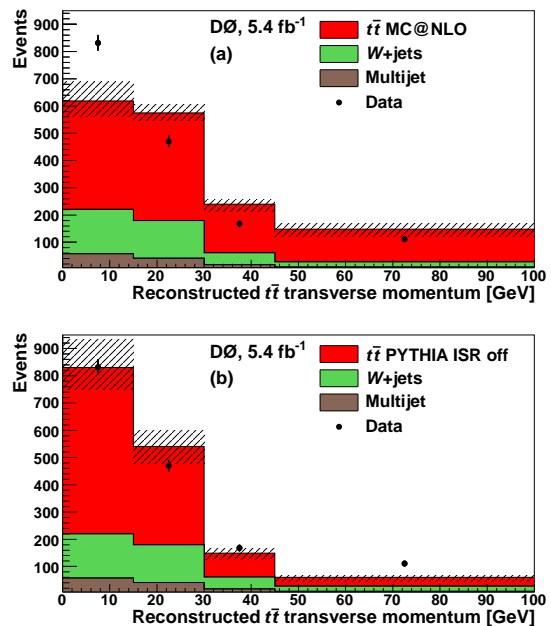

FIG. 7. The reconstructed $p_T^{t\bar{t}}$. The hatched band represents systematic uncertainties due to the jet energy scale and resolution. Data points are compared to predictions based on (a) MC@NLO and (b) PYTHIA with ISR off. Bin widths correspond to about half of the detector resolution in $p_T^{t\bar{t}}$.

that final states without extra gluons are associated with positive predicted $A_{\rm FB}$, this suggests that future simulations that predict softer $p_T^{t\bar{t}}$ spectra may also predict higher inclusive asymmetries. In PYTHIA the main effect of the additional QCD radiation is to boost the previously generated $t\bar{t}$ 4-vectors, so turning the ISR off has little effect on the inclusive production asymmetry.

Including the α_s^4 terms in the calculation of $A_{\rm FB}$ for $t\bar{t}j$ processes yields an asymmetry that is significantly less negative than at order α_s^3 [29]. Reference [30] argues that this does not affect the inclusive asymmetry in $t\bar{t}$ production.

XI. SUMMARY

We measure the forward-backward asymmetry in top quark-antiquark production, defined according to the rapidity difference between the top and antitop quarks. After background subtraction, we find a reconstructed $t\bar{t}$ asymmetry of $A_{\rm FB} = (9.2 \pm 3.7)\%$, to be compared with the MC@NLO-based prediction of $(2.4 \pm 0.7)\%$. We find no statistically significant enhancements of $A_{\rm FB}$, neither for high $m_{t\bar{t}}$ nor for large $|\Delta y|$.

The reconstructed $t\bar{t}$ asymmetry can be unfolded for acceptance and detector resolution. We apply two unfolding procedures: a four-bin unfolding and an unfolding with fine binning and explicit regularization. We argue that the latter technique is better suited to estimate migration between the regions of positive and negative

Δy and reduces the overall uncertainty on the unfolded result. The asymmetry unfolded with fine binning and explicit regularization is $(19.6 \pm 6.5)\%$, while MC@NLO predicts a value of $(5.0 \pm 0.1)\%$.

We also present an alternative approach that does not depend on a full reconstruction of the $t\bar{t}$ system — a measurement of a forward-backward asymmetry based only on the rapidity of the lepton. To avoid large acceptance corrections, we use only the region $|y_l| < 1.5$. We measure $A_{\mathrm{FB}}^l = (14.2 \pm 3.8)\%$ at the reconstruction level, to be compared to the MC@NLO-based prediction of $(0.8 \pm 0.6)\%$. Unfolding to the production level has a minimal effect on the lepton-based asymmetry, and we find $A_{\mathrm{FB}}^l = (15.2 \pm 4.0)\%$ at the production level, to be compared with the MC@NLO-based prediction of $(2.1 \pm 0.1)\%$.

The asymmetries measured in D0 data disagree with the MC@NLO-based predictions, with the most significant discrepancy above three SD. The A_{FB} value measured at production level can also be compared to other SM calculations[31], which predict similar asymmetries. We discuss some limitations of these predictions.

[1] S. Abachi *et al.* (D0 Collaboration), Phys. Rev. Lett. **74**, 2632 (1995).

[2] F. Abe *et al.* (CDF Collaboration), Phys. Rev. Lett. **74**, 2626 (1995).

[3] e.g., D. Wicke, Euro. Phys. J. C **71**, 1627 (2011).

[4] J. H. Kuhn and G. Rodrigo, Phys. Rev. Lett. **81**, 49 (1998).

[5] A. Djouadi, G. Moreau, F. Richard, and R. K. Singh, Phys. Rev. D **82**, 071702 (2010).

[6] E. L. Berger *et al.*, Phys. Rev. Lett. **106**, 201801 (2011).

[7] V. M. Abazov *et al.* (D0 Collaboration), Phys. Rev. Lett. **100**, 142002 (2008).

[8] T. Aaltonen *et al.* (CDF Collaboration), Phys. Rev. Lett. **101**, 202001 (2008).

[9] T. Aaltonen *et al.* (CDF Collaboration), Phys. Rev. D **83**, 112003 (2011).

[10] V. M. Abazov *et al.* (D0 Collaboration), Nucl. Instrum. Meth. A **565**, 463 (2006);
R. Angstadt *et al.* (D0 Collaboration), Nucl. Instrum. Meth. A **622**, 298 (2010);
M. Abolins *et al.*, Nucl. Instrum. Meth. A **584**, 75 (2008).

[11] S. Abachi *et al.* (D0 Collaboration), Nucl. Instrum. Methods Phys. Res. A **338**, 185 (1994).

[12] V. M. Abazov *et al.* (D0 Collaboration), Nucl. Instrum. Methods Phys. Res. A **552**, 372 (2005).

[13] V. M. Abazov *et al.* (D0 Collaboration), Nucl. Instrum. Methods Phys. Res. A **620**, 490 (2010).

[14] V. M. Abazov *et al.* (D0 Collaboration), accepted by Phys. Rev. D, arXiv:1101.0124 [hep-ex].

[15] V. M. Abazov *et al.* (D0 Collaboration), Phys. Rev. D **76**, 092007 (2007).

[16] S. Frixione and B. R. Webber, J. High Energy Phys. **06**, 029 (2002);
S. Frixione *et al.*, J. High Energy Phys. **08**, 007 (2003).

[17] G. Corcella *et al.*, J. High Energy Phys. **01**, 010 (2001).

[18] M. L. Mangano *et al.*, J. High Energy Phys. **07**, 001 (2003).

[19] T. Sjöstrand *et al.*, Comput. Phys. Commun. **135**, 238 (2001).

[20] S. Snyder, Doctoral Thesis, State University of New York at Stony Brook (1995).

[21] Tevatron Electroweak Working Group, CDF Collaboration, and D0 Collaboration, FERMILAB-TM-2466-E, arXiv:1007.3178 (2010).

[22] V. M. Abazov *et al.* (D0 Collaboration), Phys. Rev. D **83**, 032009 (2011).

[23] M. I. Gresham, I. W. Kim, and K. M. Zurek, Phys. Rev. D **83**, 114027 (2011).

[24] G. Bohm and G. Zech, *"Introduction to Statistics and Data Analysis for Physicists,"* Verlag Deutsches Elektronen-Synchrotron, (2010).

[25] http://root.cern.ch/root/html/TUnfold.html, *kRegModeCurvature* option.

[26] V. M. Abazov *et al.* (D0 Collaboration), Phys. Rev. Lett. **101**, 062001 (2008).

[27] M. T. Bowen, S. D. Ellis, and D. Rainwater, Phys. Rev. D **73**, 014008 (2006).

[28] P. Skands, Phys. Rev. D **82**, 074018 (2010).

[29] S. Dittmaier, P. Uwer, and S. Weinzierl, Phys. Rev. Lett. **98**, 262002 (2007).

[30] K. Melnikov and M. Schulze, Nucl. Phys. B **840**, 129 (2010).

[31] E.g., L. G. Almeida, G. Sterman, and W. Vogelsang, Phys. Rev. D **78**, 014008 (2008).